Self-Starting Capability Improvement of Single and Dual Hybrid Darrieus-Savonius VAWTs, Incorporating a Gear Mechanism

Sina Hosseini Rad, Morteza Taraghi, Farzad Ghafoorian, Mahdi Moghimi*

Department of Energy Conversion, School of Mechanical Engineering, Iran University of Science and Technology, Tehran, Iran.

A R T I C L E   I N F O

A B S T R A C T

The substantial increase in greenhouse gas emissions has catalyzed the growth of renewable energy sources. In this context, vertical axis wind turbines (VAWTs) have gained significant traction due to their numerous advantages. Notably, Darrieus VAWTs have demonstrated acceptable efficiency; however, their reliance on initial torque and challenges associated with self-starting capabilities prompted advancements in hybrid Darrieus-Savonius VAWTs. This configuration has primarily proven effective in enhancing efficiency within a low-tip speed ratio (TSR) range. However, hybrid rotors tend to experience performance degradation in high-TSR ranges. To address the performance decline observed in the high-TSR range, this study proposes an innovative solution by developing a dual-shaft hybrid rotor. This design functions as a control mechanism to prevent the angular velocity of the inner Savonius rotor from exceeding a specified threshold. For the first time, this design integrates Darrieus and Savonius rotors on a common shaft, then with two distinct rotors mounted on separate shafts. These shafts are connected through a gearless control mechanism that regulates the angular velocity of the Savonius rotor, ensuring it operates below an angular velocity of 19.79 rad/s. The findings suggest that both single and dual shaft configurations can improve rotor power coefficient (C_p) by up to 72% and 90%, respectively, in comparison to conventional rotors at a TSR of 1.4.

How to cite this article
Hosseini Rad S, Taraghi M, Ghafoorian F, Moghimi M, Self-Starting Capability Improvement of Single and Dual Hybrid Darrieus-Savonius VAWTs, Incorporating a Gear Mechanism. Modares Modares Mechanical Engineering; *2025;25(09):595-601.*

*Corresponding author's email: moghimi@iust.ac.ir
*Corresponding ORCID ID: 0000-0002-5450-3338

1- Introduction

In response to the growing concerns regarding the rise in greenhouse gas emissions, there has been a substantial increase in the adoption of renewable energy sources. Concurrently, significant advancements have been made in developing wind turbines, which serve as turbomachines for harnessing clean wind energy for electricity generation [1]. Various methods categorize wind turbines. A prominent classification approach distinguishes them based on their axis of rotation, resulting in two principal categories: horizontal axis wind turbines (HAWTs) and vertical axis wind turbines (VAWTs) [2]. VAWTs have experienced significant growth due to several advantages. These advantages include independence from the wind flow direction, lower maintenance costs compared to HAWTs, and the feasibility of installation in diverse locations, such as along highways or high-rise buildings' roofs [3]. VAWTs can be classified into two primary categories based on their aerodynamic force generation: lift-based and drag-based systems. Lift-based VAWTs, exemplified by Darrieus and Gorlov designs, are characterized by higher efficiency and a broader operating range. In contrast, drag-based VAWTs, such as Savonius models, exhibit lower efficiency and operating range; however, they possess a distinct advantage as impulse turbines, allowing for improved self-starting capabilities compared to their lift-based counterparts [4]. Multiple strategies have been proposed to enhance the efficiency of Darrieus VAWTs and their self-starting capabilities. These include the optimization of blade geometry, the implementation of external flow control devices, and the design of hybrid or multi-stage turbine systems [5], [6], [7]. Integrating Savonius VAWTs with Darrieus VAWTs to create hybrid turbine designs has become a prevalent approach to enhancing efficiency within the low tip-TSR range. This combined design also contributes to improved self-starting capabilities. However, it has been observed that this approach results in a decrease in the power coefficient ( ) at the high-TSR range [8]. Roshan et al. [9] demonstrated that the hybrid Savonius-Darrieus VAWT increased from 0.01 to 0.2 at the initial tip speed TSR. However, they also noted a significant decline in efficiency at the high-TSR range. Abdelsalam et al. [10] demonstrated that the hybrid Savonius-Darrieus VAWT performs better than the conventional Darrieus VAWT. This enhancement not only broadened the operational range, increasing TSR from 3.5 to 4 but also resulted in a 23% improvement in efficiency. The experimental findings of Pallotta et al. [11] indicate that the enhancement of efficiency within the hybrid configuration has yielded improvements of up to 80% in the low-TSR range. This enhancement has contributed to an improved self-starting capability. However, at the high-TSR range, the inefficiency of this configuration, in comparison to the conventional Darrieus vertical VAWT, remains a significant concern. Despite several optimizations implemented in hybrid configurations, the challenge of efficiency loss persists in the high-TSR range when both Darrieus and Savonius turbines are installed on a shared shaft without an integrated control system. This issue primarily stems from aerodynamic instabilities [12].

The Darrieus-Savonius hybrid VAWT has demonstrated a significant ability to enhance the efficiency of Darrieus VAWTs, particularly within the low-TSR range. This improvement has resulted in a superior self-starting capability compared to conventional Darrieus rotors. However, challenges have been identified concerning the efficiency of single-shaft hybrid Darrieus-Savonius rotors at high-TSR ranges. Specifically, the drag-based Savonius rotors, designed for low angular velocities, negatively impact the performance of Darrieus rotors in high-TSR ranges due to vortex shedding affecting the outer Darrieus rotor field. Consequently, this study proposes an innovative approach, which, to the best of our knowledge, is the first time that Savonius and Darrieus rotors are mounted on two separate shafts equipped with a gearless control mechanism instead of a single shaft. This design prevents the Savonius rotor from exceeding a

Table 1. Hybrid Darrieus-Savonius VAWT Dimensions.

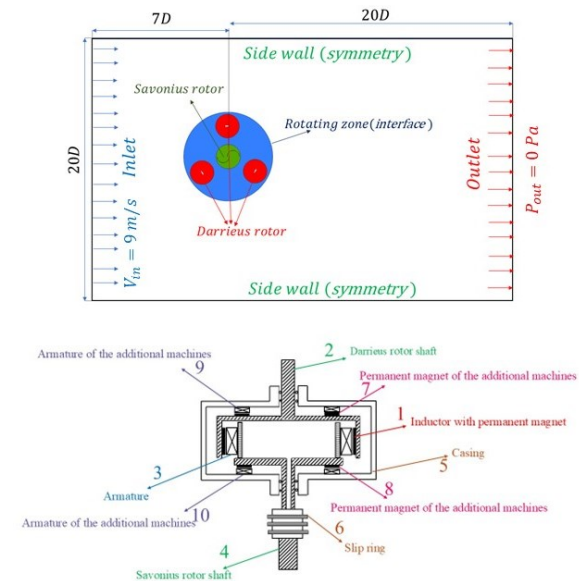| Parameter	Darrieus VAWT	Savonius VAWT
Number of blades	3	2
Rotor diameter	1030(mm)	370(mm)
Blade chord length	85.8 (mm)	-
Overlap size	-	30(mm)
Airfoil profile	NACA0021	-

Fig.1 a) Hybrid rotor configuration and computational domain, b) Sketch of transmission system

specific angular velocity, wherein drag-based rotors exhibit inefficiency. The rotational speed of the Savonius rotor is regulated via this gearless mechanism, aiming to minimize efficiency losses and optimize the aerodynamic performance of the rotor within the high-TSR range and provide higher C_p values and better aerodynamic behavior within high-TSR range compared to single-shaft hybrid rotors.

2- Geometry Description

This simulation features a hybrid Darrieus-Savonius VAWT. The model utilized for the Darrieus rotor was developed by Castelli et al. [13], while the Savonius rotor employed the model created by Wenehenubun et al. [15]. Table 1 details the dimensions of both turbines, and Figure 1 presents the associated schematic of the transmission mechanism. For the domain dimensions, we need to select appropriate dimensions to ensure fully developed flow both upstream and downstream of the rotor, while preventing reverse flow from the sidewalls. Therefore, the inlet and outlet from the rotor center are set at 7D and 20D from the rotor center, respectively. Additionally, the width of the domain is set to 20D to prevent blockage effects and the negative effect of accelerated flow from the lateral walls.

Figure 1 illustrates that the drivetrain transmission system is centrally located along the rotational axis of the hybrid co-axial rotor, enabling the independent and unrestricted accommodation of the inner and outer rotor shafts. This gearless transmission mechanism comprises an inductor equipped with permanent magnets (1) integrated with the primary rotor's shaft, which features a Darrieus rotor design (2). The armature (3) is connected to the secondary rotor's shaft, characterized as a Savonius rotor (4). Both shafts possess the capability to rotate independently within their respective casing (5). Slip rings (6) are utilized to provide power to the armature winding (3). Furthermore, the system incorporates two low-power synchronous electric machines outfitted with permanent magnets (7 and 8) mounted on the rotors, while the armatures (9 and 10) reside within the casing, facilitating electromagnetic coupling between the dynamic rotors and

their surrounding casing (5). This setup stabilizes the hybrid CR-VAWT by adjusting the torque between the two rotors, enabling one to assist the other. The system allows one rotor to act as a motor and the other as a generator, drawing power from each other and requiring minimal external input. These motors/generators also help with initial rotor acceleration.

3- Governing Equation

The Unsteady Reynolds-averaged Navier-Stokes (URANS) equation is essential for analyzing fluid dynamics around blades and buckets. It efficiently examines unsteady, turbulent flow, clarifying the relationship between pressure and velocity. It utilizes a time-averaging approach to quantify turbulence based on Newton's laws of motion and momentum conservation [15].

$$\frac{\partial \overline{u_i}}{\partial x_i} = 0 \tag{1}$$

$$\frac{\partial \overline{u_i}}{\partial t} + \overline{u_j}\frac{\partial \overline{u_i}}{\partial x_j} = -\frac{1}{\rho}\frac{\partial \overline{p}}{\partial x_i} + \nu \frac{\partial^2 \overline{u_i}}{\partial x_j^2} - \overline{u_j'}\frac{\partial \overline{u_i'}}{\partial x_j} \tag{2}$$

The continuity equation, represented as Equation 1, signifies mass conservation within a fluid domain. Equation 2 details the momentum equation's dynamics, encompassing the principles of force, mass, and acceleration. The variables $\overline{u_i}$ (m/s) and $\overline{u_j}$ (m/s) reflect the initial velocity components in a Cartesian framework, while the fluctuating velocities u_i' (m/s) and u_j' (m/s) capture turbulence and uncertainties. Furthermore, mean pressure $\overline{p}$ (N/m²), density ρ (kg/m³), and kinematic viscosity ν (m²/s) define essential fluid properties. Notably, the Reynolds stress $u_i'u_j'$ reveals the correlation between fluctuating variables across velocity components, offering insights into the complex momentum transformations induced by turbulence.

For turbulent flow modeling, the $k - \omega$ SST model, which integrates $k - \varepsilon$ and $k - \omega$ models, provides enhanced predictions regarding the aerodynamic behavior of blades. This model effectively captures flow characteristics in both near-wall regions, similar to the $k - \omega$ model, and demonstrates sufficient accuracy for far-field regions, which is a hallmark of the $k - \varepsilon$ model. Therefore, it represents the optimal choice for turbomachinery applications, as it adeptly accommodates flow behavior in both proximity to walls and within the broader flow field. The formulation of the SST $k - \omega$ model is as follows [15]:

$$\rho \frac{d}{dt}(k) + \rho \nabla \cdot [k(\vec{u} - \overrightarrow{u_g})] = \nabla \cdot \left[\left(\mu + \frac{\mu_t}{\sigma_k}\nabla k\right)\right] + G_k - Y_k \tag{3}$$

$$\rho \frac{d}{dt}(\omega) + \rho \nabla \cdot [\omega(\vec{u} - \overrightarrow{u_g})] = \nabla \cdot \left[\left(\mu + \frac{\mu_t}{\sigma_\omega}\nabla \omega\right)\right] + G_\omega - Y_\omega \tag{4}$$

The variables $Y_k \left(\frac{kg}{m^3 \cdot s^3}\right)$ and $G_k \left(\frac{kg}{m^3 \cdot s^3}\right)$ represent dissipation and turbulence kinetic energy production, respectively. $G_\omega \left(\frac{1}{m^3 \cdot s^3}\right)$ and $Y_\omega \left(\frac{1}{m^3 \cdot s^3}\right)$ denote ω specific generation and dissipation, respectively. Wind turbines' power and torque coefficients can be analyzed to assess their efficiency.

$$C_p = \frac{P}{1/2\rho A V^3} \tag{5}$$

$$C_m = \frac{P}{1/2\rho D^2 H V^2} \tag{6}$$

where ρ is wind density equals to 1.225 kg/m3 and A is assumed as swept area of the rotor .

In addition, turbine TSR could be calculated from:

$$TSR = \frac{R\Omega}{V} \tag{7}$$

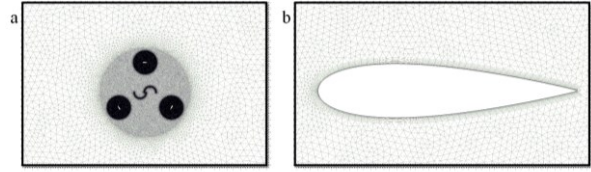where Ω is rotational speed, and V is wind velocity.

Fig.2 Mesh structure a) around rotor b) around airfoil

Table 2. Grid specification and mesh independence study summary

Grid properties	Grid 1	Grid 2	Grid 3	Grid 5
Number of elements $\times 10^3$	220	430	640	917
airfoil element size (mm)	0.05	0.03	0.015	0.012
Bucket element size (mm)	0.85	0.64	0.42	0.21
Number of inflation layers	12	14	16	18
Darrieus first layer thickness(mm)	0.029	0.024	0.019	0.015
inflation growth rate	1.2	1.15	1.1	1.05
Maximum skewness	0.946	0.948	0.939	0.931
Averaged y^+	1.37	0.89	0.85	0.72
C_p	0.185	0.184	0.183	0.182

4- Grid and Time Study

The present simulation uses ANSYS-Mesh for domain discretization. A structured grid of quadrilateral elements is the boundary layer mesh to enhance accuracy near the blade wall, reducing sharp flow variations. Unstructured triangular elements are operated in the rotating and stationary zones. Incremental grid coarsening materializes from the airfoil surfaces to the rotor-stator interface. A non-conformal mesh with specific sizing is implemented for the sliding interface and designed to improve grid density and instability calculation accuracy. Figure 2 illustrates the mesh distribution around the blades and rotors. The specifications for the generated mesh of the hybrid rotor are presented in Table 2.

As indicated in Table 2, the average value of Y^+, which characterizes the dimensionless distance perpendicular to the wall and correlates with the boundary layer's thickness, for all cases, except for Case 1, was below 1, which falls within an acceptable range. Furthermore, the maximum skewness value, one of the primary quality measures for the mesh, ideally approximating 0.95 for the generated mesh, was also deemed acceptable. Additionally, the variations in C_p values across different mesh configurations did not exhibit significant differences, suggesting that the mesh's number or density did not influence the solutions and results obtained. To enhance the comprehension of the findings from the mesh independence study, the results concerning the torque coefficient throughout a complete cycle for various mesh configurations related to Darrieus rotors are presented in Figure 3.

Figure 3 further corroborates the independence of the results from the number of meshes, as the maximum difference in the torque coefficient values among the various cases remains below 10%, with an approximate difference of 7%. Additionally, referring to these results and Table 2, it is observed that the variance between the highest and lowest values of the power coefficient, particularly between cases 1 and 3, is approximately 2%. Consequently, these findings substantiate the accuracy of the mesh study.

Ensuring data independence at each incremental time step is a critical challenge in CFD projects, especially for VAWTs due to rapid flow changes around the blades at low TSRs. The high vorticity gradient at these TSRs complicates maintaining data independence. Therefore, careful attention is essential in the CFD simulation of VAWTs to ensure data independence across time steps. Figure 4 shows the averaged values for grid case 2 regarding time independence and step sensitivity analysis, with a flow time of 0.2 seconds. It presents results for four different time step sizes: 0.001 s, 0.0005 s, 0.00025 s, and

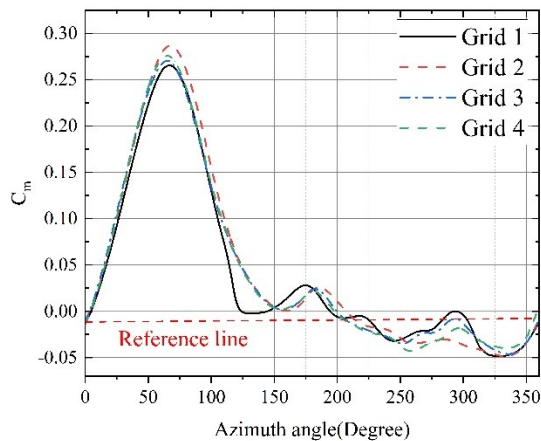0.00005 s, corresponding to $\Delta\theta$ values of 2°, 1°, 0.5°, and 0.1°, based on a TSR value of 2.

Fig.3 One blade torque coefficient as function of azimuth angle in a complete rotation at TSR = 1.4.
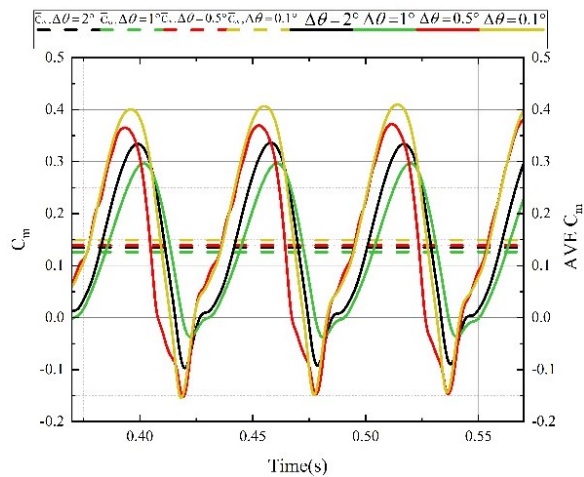

Fig.4 Variation of torque coefficient in relation to time for different time steps and time step sensitivity analysis at TSR = 2.

Figure 4 demonstrates that changes in show a consistent pattern across all time intervals. The data indicates that variability in average is minimal, with only a 1% relative difference between angular adjustments of 0.1° and 2°. This observation reinforces the solution's independence from the time step, further corroborating recent findings in CFD.

5- Solver setting

The investigation utilized Ansys Fluent 2021 R2 to perform numerical simulations of transient, unsteady flow around turbine blades. A pressure-based model was selected to address the momentum and continuity equations, which are suitable for the incompressible nature of air at low velocities. The SIMPLE (Semi-Implicit Method for Pressure-Linked Equations) scheme was employed to accurately resolve the challenges associated with velocity–pressure interactions, enabling independent corrections of momentum and pressure. To ensure computational accuracy, the second-order upwind method was applied to discretize the governing equations for pressure, momentum, turbulence kinetic energy, and specific dissipation rate. Convergence analysis was conducted using the torque coefficient, defined as convergent when the difference between periods fell below 1%. A convergence threshold was set at 10^{-6}, with 30 iterations conducted per time step. The simulation primarily focused on analyzing torque fluctuations and output power trends. Results were deemed invalid if

torque and power fluctuations did not exhibit a consistent trend. Upon achieving stabilization, the average power was employed to calculate
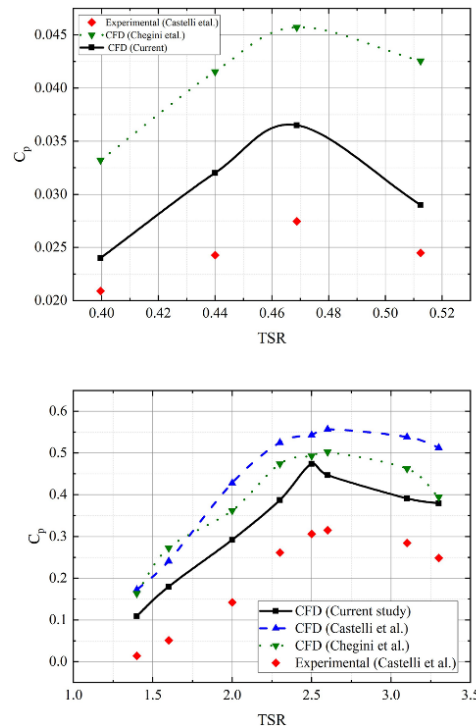

Fig.5 CFD model validation a) Darrieus rotor b) Savonius rotor

the C_p, and subsequently, a rotor cycle was assessed for torque on an individual blade.

6- Model Validation

This study used a dual-validation process to independently validate the Darrieus and Savonius rotors, assessing rotor performance under different operating conditions and TSRs, and confirming the validity of the hybrid configuration. To validate the performance of the Darrieus rotor, the model developed by Castelli et al. [13] has been utilized as a reference. The boundary conditions have been meticulously adhered to, with the inlet velocity set at 9 m/s and the flow exiting the domain at a pressure outlet, maintaining a zero-gauge pressure to the atmosphere. Additionally, a no-slip condition has been implemented for the walls. Similarly, the Savonius rotor has been analyzed, applying corresponding boundary conditions as outlined in the study by Wenehenubun et al. [14], with an assumed inlet velocity of 10 m/s. The validation results are presented in Figure 5. To ensure the precision of the validation results, the recent findings have been compared not only to previous experimental outcomes but also to the earlier CFD results established by Chegini et al. [16].

As illustrated in Figure 5a, the CFD results within the range of TSRs from 1.4 to 3.3 correspond to angular velocities ranging from 24.92 to 57.34 rad/s. These findings indicate a satisfactory correlation with previous CFD and experimental results. Furthermore, the recent outcomes have been compared with earlier CFD data, revealing not only an acceptable level of agreement but also a closer alignment with the experimental results. This trend is similarly evident in Figure 5b, where the current CFD results are significantly more aligned with the experimental outcomes when compared to the prior simulation, resulting in a decrease in the error percentage. For Savonius rotor, the percentage difference between the recent CFD and previous experimental results at a TSR=0.4 is less than 20%, which is deemed acceptable for validation purposes. Furthermore, the Betz limit has been obeyed for both Darrieus and Savonius rotors. Specifically, at TSR values of 2.6 and 0.7, respectively, the power coefficient for

these rotors began to decline, indicating a cessation of its upward trend. The results obtained indicate that the CFD simulation has been
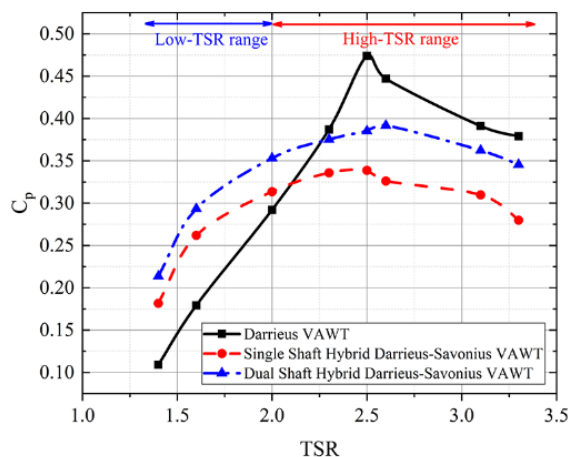

Fig.6 Performance map for conventional and hybrid cases

validated. The discrepancies observed compared to the experimental results can be attributed to the geometric simplifications, the 2D modeling approach, and the assumptions associated with the URANS method.

7- Results and Discussion

In this section, we examine not only the conventional Darrieus VAWT but also a hybrid Darrieus-Savonius VAWT model. In the first hybrid configuration, both the Savonius and Darrieus rotors are mounted on a common shaft, rotating at an identical angular velocity. In the second configuration, each rotor is positioned on separate shafts. The angular velocity of the Savonius rotor is regulated through a gear mechanism to ensure that the angular velocity of the Savonius rotor does not exceed a predetermined threshold of 19.79 rad/s. Each turbine performance map is shown in Figure 6.

According to Figure 6, the hybrid configuration, whether implemented as a single shaft or a dual shaft system, has significantly enhanced the efficiency of the rotor in the low TSR range. Specifically, at a TSR of 1.4, the single-shaft and dual-shaft hybrid turbines have achieved 72% and 90% efficiency (C_p) enhancement, respectively compared to the conventional Darrieus rotor. This improvement also indicates a notable enhancement in the self-starting capability of the rotor. Integrating the Darrieus rotor with the Savonius rotor, whether configured on a single shaft or arranged separately, significantly enhances efficiency and self-starting capability in hybrid systems. Furthermore, the dual-shaft configuration has effectively mitigated the potential limitations commonly associated with commercial single-shaft hybrid Darrieus-Savonius VAWTS, especially in the high-TSR range. It is recognized that the efficiency of hybrid turbines in the high-TSR range is reduced compared to conventional rotors. However, this limitation has been partially addressed by decoupling the rotor shafts and employing a gearless mechanism to regulate the angular velocity of the Savonius rotor. The dual-shaft system functions as a control mechanism through the utilization of gearing, effectively preventing excessive increases in the angular velocity of the Savonius rotor. It maintains the angular velocity at 19.79 or a TSR of 0.37. The design of the Savonius VAWT is inherently tailored for operation within a low-TSR range without efficiency drop. The dual design serves to restrict the Savonius rotor from entering the high-TSR range operating conditions and consequently facing efficiency challenge. In the high-TSR range, specifically at a TSR of 2.5, the single-shaft rotor demonstrated a 30% reduction in C_p compared to the conventional configuration. Conversely, the dual-shaft configuration, equipped with control mechanisms, exhibited superior performance with only a 20%

reduction in C_p compared to the conventional case. This observation highlights the enhancements achieved in the hybrid rotor design with
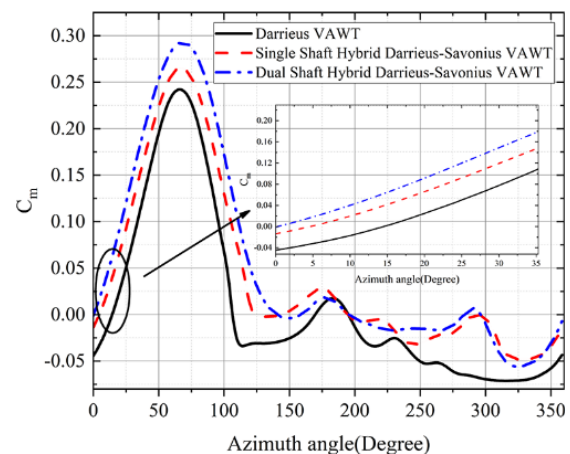

Fig.7 Torque coefficient as a function of azimuth angle for a single rotor blade
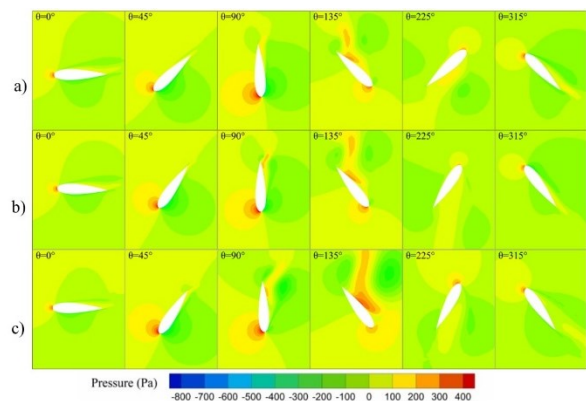

Fig.8 Pressure field around a single blade a) Dual shaft b) Single shaft c) Conventional rotors

control mechanisms, particularly within the high-TSR range. It should be emphasized that the dual-shaft hybrid rotor enhances the aerodynamic response and C_p values compared to the single-shaft hybrid rotor across both TSR ranges; therefore, the dual-shaft configuration is suggested instead of the single-shaft.

Based on Figure 7, which illustrates the rotor torque coefficient of a single rotor blade throughout a complete rotation at various azimuth angles, it is evident that the self-starting capability of the rotor with hybrid configurations has improved. Notably, the dual shaft configuration demonstrates superior performance in the azimuth angle range from 0° to 100° compared to the single shaft configuration. Specifically, at the starting point of the rotor, the torque coefficient at the azimuth angle of 0° has reached a value of 0, thereby effectively addressing the self-starting challenges associated with the rotor.

Based on Figure 8, the analysis indicates that the pressure gradient at the leading edge of the blade remains consistent across all three configurations at an azimuth angle of 0°. However, as the rotor transitions towards the upwind region at an azimuth angle of 45°, the pressure gradient on the suction side of the blade experiences an increase of up to 200 Pa. Notably, in the dual shaft configuration, the positive pressure layer completely adheres to the suction side, which has enhanced the self-starting capability of the system. In other words, when high-pressure zones accumulate at the leading edge of the rotor at the upper blade surface, which aligns with both the rotor's direction of rotation and the torque arm, this advantageous pressure zone serves to enhance the equivalent torque and improve the system's self-starting capability. The accumulation of a high-pressure area and a

positive pressure value of 300 Pa on the suction side of both dual-shaft and single-shaft rotor blades at an azimuth angle of 90° was observed to be greater than that of the conventional rotor configuration. This high-pressure zone aligns with rotor rotation, resulting in an increase in equivalent torque compared to the conventional rotor. This observation underscores the effective application of hybrid configurations. In addition, the conventional rotor configuration exhibits a more significant unfavorable positive pressure gradient at the trailing edge, particularly on the pressure side. This phenomenon contrasts with the direction of rotor rotation and the torque arm, leading to a reduction in equivalent torque and a subsequent decline in self-starting capability. This effect is notably less pronounced in hybrid rotor configurations when compared to the conventional case, which resulted in equivalent torque and self-starting capacity improvement. The accumulation of an unfavorable positive pressure gradient on the pressure side of the conventional rotor blade at an azimuth angle of 135° is entirely evident. The development of a high-pressure zone of 250 Pa on the conventional rotor blade pressure side occurs in a direction that is contrary to the rotor's rotation. This phenomenon significantly reduces the equivalent torque compared to hybrid configurations. In contrast, hybrid configurations show a decrease in unfavorable pressure gradient on the pressure side, which results in an improved self-starting capability. Additionally, as the rotor continues to rotate and reaches an azimuth angle of 225°, the accumulation of the positive pressure gradient at the blade's leading edge in hybrid configurations is reduced and facilitates rotor rotation. At an azimuth angle of 315°, where the rotor is transitioning back to the windward region, there is a notable accumulation of positive pressure at the leading edge across all configurations. This accumulation has resulted in a decrease in torque for each configuration. Furthermore, the positive pressure gradient around the leading edge of the conventional rotor blade is fully developed, which has led to a decline in its aerodynamic performance. Overall, the evidence presented by the pressure field corroborates the torque coefficient results observed at various azimuth angles.

The observations in Figure 9 indicate that incorporating a Savonius turbine in the hybrid configuration induces vorticity from the bucket tips to the trailing edges of the Darrieus rotor blades. This suggests that the vorticity field for the Darrieus turbine remains consistent across different azimuth angles. At an azimuth angle of 0°, the vorticity generated at the convex portion of the Savonius rotor buckets has minimal aerodynamic impact, limiting its expansion. However, as the turbine rotates, the vorticity field expands significantly, peaking at an azimuth angle of 225°. At this point, the vorticity becomes substantial, affecting the Darrieus blades. The resulting vortex flow increases drag on the buckets' convex section and the Darrieus blades' pressure side, thereby reducing the efficiency of the hybrid rotor. The arrangement of the gear mechanism, coupled with the regulation of the rotor's rotational speed and the assessment of position variation between the Savonius and Darrieus rotors, has led to a significant reduction in the development of vorticity and its intensity. Notably, the diminution of vorticity magnitude surrounding the buckets, particularly in both the concave and convex regions, is evident at an azimuth angle of 225°.

In general, the vortex shedding from the tips of the Savonius rotor and its subsequent impact on the Darrieus rotor is an unavoidable phenomenon. This occurs particularly when the Savonius rotor is mounted on a shared shaft with the Darrieus rotor, leading to an increase in the angular velocity of the Savonius rotor in conjunction with the Darrieus rotor. Consequently, the adverse effects of vortex shedding on the Darrieus rotor are aggravated. However, by implementing control mechanisms, the angular velocity of the Savonius rotor can be restricted, preventing it from exceeding that of the Darrieus rotor. As a result, the development of vortices and their detrimental impact on the Darrieus rotor are significantly diminished.
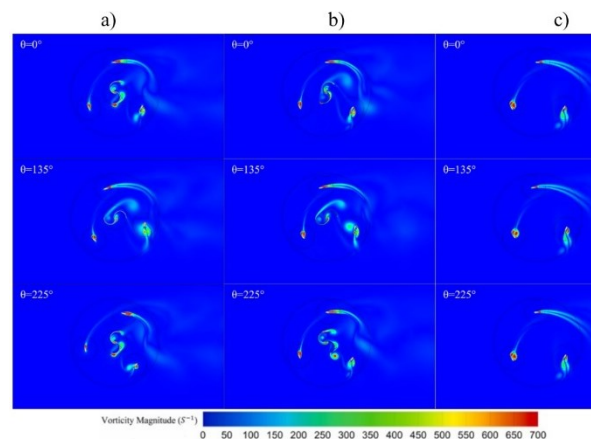

Fig.9 Vorticity field around a single blade a) Dual shaft b) Single shaft c) Conventional rotors

8- Conclusion

This study examines a hybrid Darrieus-Savonius VAWT configuration designed to enhance the self-starting capability of the conventional Darrieus turbine. The performance map results revealed that Savonius drag-based VAWTs are typically engineered to function effectively within low-TSR ranges, where their efficiency tends to decline as the TSR increases due to rising angular velocity. Implementing a hybrid configuration utilizing two distinct shafts, coupled with a geared mechanism to regulate the rotational velocity of the Savonius rotor, not only improved the rotor's efficiency in the low-TSR range but also addressed the efficiency loss encountered in the high-TSR range. This advancement is attributed to the gear mechanism, which effectively limited the rotational velocity of the Savonius rotor to 19.79 rad/s, thereby enhancing overall system performance compared to a conventional single-shaft configuration. The results of the torque coefficient at different azimuth angles demonstrated that the dual shaft configuration successfully increased the torque coefficient at an azimuth angle of 0 from negative values to zero. This improvement significantly enhances the self-starting capability of the hybrid turbine, eliminating the need for initial torque. This performance enhancement was also validated by analyzing the pressure and vorticity fields. Specifically, single and dual shaft hybrid rotors improve the C_p within the low-TSR range, achieving values of 72% and 90% respectively, compared to conventional designs. This enhancement in the low-TSR range highlights the efficiency of hybrid rotors, particularly in their self-starting capabilities, with the dual-shaft hybrid rotor demonstrating superior performance. Additionally, within the high-TSR range, the dual-shaft rotor equipped with a control mechanism shows a 10% improvement at a TSR of 2.5 compared to the single-shaft hybrid rotor, indicating the better aerodynamic performance of the dual-shaft rotor compared to the commercial design of single-shaft rotors.

For future studies, it is recommended to investigate the dynamic mesh approach for the inner Savonius rotor while avoiding the specification of angular velocity and employing a sliding mesh methodology. The dynamic mesh approach allows the Savonius rotor to operate freely, thereby providing deeper insights into the performance of control mechanisms.

Ethical Statement

The content of this manuscript is original, based on the authors' research, and has not been published or submitted elsewhere, either in Iranian or international journals

Conflict of interest

The authors declared that they have no conflicts of interest to this work.

References

[1]   M. Mehrpooya, M. Mohammadi, and E. Ahmadi, "Techno-economic-environmental study of hybrid power supply system: A case study in Iran," Sustainable Energy Technologies and Assessments, vol. 25, pp. 1–10, Feb. 2018, doi: http://doi.org/10.1016/j.seta.2017.10.007.

[2]   H. Seifi Davari, M. Seify Davari, R. M. Botez, and H. Chowdhury, "Advancements in Vertical Axis Wind Turbine Technologies: A Comprehensive Review," Arabian Journal for Science and Engineering, pp. 1–48, 2024.

[3]   A. G. Chitura, P. Mukumba, and N. Lethole, "Enhancing the Performance of Savonius Wind Turbines: A Review of Advances Using Multiple Parameters," Energies, vol. 17, no. 15, 2024, doi: http://doi.org/10.3390/en17153708.

[4]   A. Rosato, A. Perrotta, and L. Maffei, "Commercial Small-Scale Horizontal and Vertical Wind Turbines: A Comprehensive Review of Geometry, Materials, Costs and Performance," Energies, vol. 17, no. 13, p. 3125, 2024.

[5]   A. Tayebi and F. Torabi, "Flow control techniques to improve the aerodynamic performance of Darrieus vertical axis wind turbines: A critical review," Journal of Wind Engineering and Industrial Aerodynamics, vol. 252, p. 105820, Sep. 2024, doi: http://doi.org/10.1016/j.jweia.2024.105820.

[6]   D. H. Seifi, S. Kouravand, and I. Khatami, "Improving the performance self-starting of the vertical axis wind turbine using porous blade," 2020.

[7]   A. JALALI and M. ZAMANI, "Effect of blade angle of attack on the performance of the darius j-shaped vertical axial wind turbine," 2020.

[8]   J. Pan, C. Ferreira, and A. Van Zuijlen, "Performance analysis of an idealized Darrieus–Savonius combined vertical axis wind turbine," Wind Energy, vol. 27, no. 6, pp. 612–627, Jun. 2024, doi: http://doi.org/10.1002/we.2904.

[9]   A. Roshan, A. Sagharichi, and M. J. Maghrebi, "Nondimensional parameters' effects on hybrid Darrieus–Savonius wind turbine performance," Journal of Energy Resources Technology, vol. 142, no. 1, p. 011202, 2020.

[10]   A. M. Abdelsalam, "Performance study on a modified hybrid wind turbine with twisted Savonius blades," Energy Conversion and Management, 2021.

[11]   A. Pallotta, D. Pietrogiacomi, and G. P. Romano, "HYBRI – A combined Savonius-Darrieus wind turbine: Performances and flow fields," Energy, vol. 191, p. 116433, Jan. 2020, doi: http://doi.org/10.1016/j.energy.2019.116433.

[12]   T. Wakui, Y. Tanzawa, T. Hashizume, and T. Nagao, "Hybrid configuration of Darrieus and Savonius rotors for stand-alone wind turbine-generator systems," Electrical Engineering in Japan, vol. 150, no. 4, pp. 13–22, 2005.

[13]   M. Raciti Castelli, A. Englaro, and E. Benini, "The Darrieus wind turbine: Proposal for a new performance prediction model based on CFD," Energy, vol. 36, no. 8, pp. 4919–4934, Aug. 2011, doi: http://doi.org/10.1016/j.energy.2011.05.036.

[14]   F. Wenehenubun, "An Experimental Study on the Performance of Savonius Wind Turbines Related With The Number Of Blades," Energy Procedia, p. 8, 2015.

[15]   A. M. Chowdhury, H. Akimoto, and Y. Hara, "Comparative CFD analysis of Vertical Axis Wind Turbine in upright and tilted configuration," Renewable Energy, vol. 85, pp. 327–337, Jan. 2016, doi: http://doi.org/10.1016/j.renene.2015.06.037.

[16]   S. Chegini, M. Asadbeigi, F. Ghafoorian, and M. Mehrpooya, "An investigation into the self-starting of darrieus-savonius hybrid wind turbine and performance enhancement through innovative deflectors: A CFD approach," Ocean Engineering, vol. 287, p. 115910, Nov. 2023, doi: http://doi.org/10.1016/j.oceaneng.2023.115910.